Arab J Sci Eng (2017) 42:4427–4437
DOI 10.1007/s13369-017-2526-y

RESEARCH ARTICLE - CHEMISTRY

Synthesis of Fe_3Al Intermetallic Compound by Mechanical Alloying

Deepankar Panda[1] · **Pallabi Bhuyan**[1] · **Lailesh Kumar**[1] · **Syed Nasimul Alam**[1]

Received: 29 September 2016 / Accepted: 10 April 2017 / Published online: 2 May 2017

Abstract In the present work, nanostructured Fe_3Al intermetallic compound has been synthesized by mechanical alloying (MA) of $Fe_{75}Al_{25}$ powder milled for 40 h followed by heat treatment at 1100 °C for 2 h in Ar atmosphere. The structural evolution of the $Fe_{75}Al_{25}$ powder during MA and subsequent isothermal annealing was analyzed using X-ray diffraction (XRD). After 40 h of milling, a disordered Fe(Al) solid solution is formed. On annealing, the Fe(Al) solid solution undergoes an ordering transformation resulting in the formation of ordered $D0_3$-Fe_3Al. The presence of the (111) superlattice peak in the XRD plot of the annealed powder is a direct evidence of the ordered arrangements in the alloy. A shallow exothermic peak below 600 °C in the DSC plot of the 40-h milled powder also confirms the formation of ordered $D0_3$-Fe_3Al. The EDX analysis of the $Fe_{75}Al_{25}$ powder milled for various periods of time confirmed the gradual increase in Al diffusion in the Fe particles. The diffusion process of Al in Fe was analyzed using the elemental maps of Fe and Al in the $Fe_{75}Al_{25}$ powder milled for various periods of time. HRTEM images confirmed that the Fe_3Al synthesized by MA is <15 nm in size.

Keywords Mechanical alloying (MA) · Intermetallics · Iron aluminides · Diffusion · HRTEM

✉ Syed Nasimul Alam
syedn@nitrkl.ac.in; nasimulalam@yahoo.com

[1] Department of Metallurgical and Materials Engineering, National Institute of Technology Rourkela, Rourkela, Orissa 769008, India

1 Introduction

An intermetallic is a compound consisting of two or more metals in a proper stoichiometric ratio. Intermetallic compounds have been used to strengthen conventional metals and alloys. However, more recently they have attracted great interest as monolithic structural materials for high-temperature applications. The demand for materials having high stiffness and strength at higher operating temperatures has led to an enormous growth of interest in intermetallics, especially silicides and ordered intermetallics such as aluminides. Among the several intermetallic compounds, available iron aluminide (Fe_3Al) has been frequently considered for high-temperature structural applications because of their unique physical and mechanical properties. Fe_3Al has a high melting point (1540 °C), high hardness (338 HV), low density (6.72 g/cc) and good oxidation and corrosion resistance [1–3]. Fe_3Al has gained noticeable attention as an intermetallic compound that could be used for high-temperature structural applications owing to their outstanding corrosion and sulfidation resistance and excellent wear resistance. However, due to its poor ductility and fracture toughness, the use of Fe_3Al is not preferred at low temperatures. At a lower temperature, Fe_3Al has an ordered atomic arrangement, and its brittle nature can be attributed to the poor dislocation motion in a highly ordered lattice [4–7]. Iron aluminide (Fe_3Al) is one of the most popular intermetallic compounds. Depending upon the chemical composition, Fe_3Al has several forms. Figure 1a shows the Fe–Al binary phase diagram [8]. According to the phase diagram at lower concentrations of Al (18–20 at.%), α, a disordered solid solution of Al in Fe, is stable. With the increase in Al concentration two ordered phases of iron aluminide, $D0_3$, and B2 are stable. From the binary phase diagram of the Fe–Al system, it is evident that there are equilibrium phases such as the disordered solid solution (α),

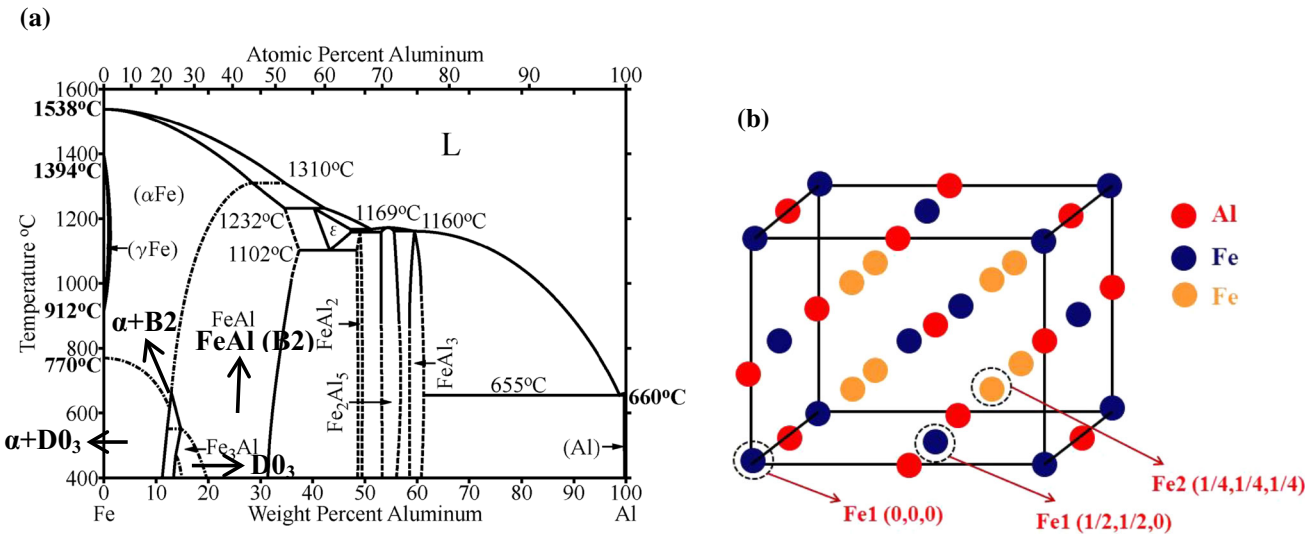

Fig. 1 **a** Binary phase diagram of the Fe–Al system [7]. **b** $D0_3$ crystal structure of Fe_3Al

Fe_3Al with imperfectly ordered B2 structure, ordered Fe_3Al with $D0_3$ structure and two-phase regions like $\alpha + D0_3$ and $\alpha + B2$. These phases are stable within a wide compositional range. From the phase diagram, it is evident that at room temperature the $D0_3$ crystal structure of the Fe_3Al intermetallic compound is stable in the composition range of around 22–37 at.% Al and can be transformed to the B2 type crystal structure when annealed above the $D0_3$–B2 transition temperature (T_c) [8,9]. The transition temperature for B2 $\Leftrightarrow$ $D0_3$ and vice versa at the stoichiometric composition of Fe_3Al is approximately 550 °C. This is the critical temperature for ordering. The Fe_3Al transforms from an ordered $D0_3$ crystal structure to a defective ordered B2 crystal structure above this temperature. With the rise in Al concentration (above 37 at.% Al) at room temperature, the B2 type crystal structure becomes more stable. FeAl intermetallic compound has a B2 type crystal structure. The concentration of Al in FeAl varies from approximately 37–50 at.% Al [10–12].

Figure 1b shows the $D0_3$ crystal structure of Fe_3Al. It is evident from the figure that there are two types of Fe atoms. One named as Fe1 has tetrahedral symmetry and can be indexed as (0, 0, 0) and (1/2, 1/2, 0). The other type of Fe atoms named as Fe2 has cubic point symmetry and can be indexed as (1/4, 1/4, 1/4). Fe1 atoms have a magnetic moment similar to FCC Fe crystal, whereas Fe2 atoms have a magnetic moment similar to BCC Fe crystal. Al atoms are usually present at the body center position and can be indexed as (1/2, 1/2, 1/2). The $D0_3$ superlattice crystal structure is comprised of eight B2 type superlattices stacked with each other, but with an alternating Fe and Al as body centered atoms. Al atoms are positioned in such a way that the spacing between the Al atoms can be maximized with the minimization of the energy. The $D0_3$ structure can be viewed as comprised of four nonequivalent interpenetrating FCC sublattices. The production of intermetallic compounds is more difficult as compared to any other alloy due to their high melting points. Mechanical alloying (MA) is the most popular and economically viable process for the development of intermetallic compounds. During milling, large plastic deformations occur. This leads to a high defect density which initiates the transformation to disordered and amorphous state [13,14].

MA of Fe–Al system has been reported earlier in the literature by several researchers. Murty and Ranganathan [15] have reported that MA is a very promising technique for the synthesis of intermetallics. Among all the intermetallic compounds that have been synthesized by MA, the aluminides have so far received major attention. A large volume of work is available in the literature on the synthesis of Ni, Ti and Fe-aluminides by MA. Oleszak and Shingu [16] have reported on the MA of Fe–Al powder mixtures in the composition range Fe-10, 20, 30, 20 and 50 at.% Al. They have reported on the morphological transition of the milled powder from a flake-like shape in the initial stages to a spherical shape during the final stages after the subsequent isothermal annealing of the milled powder. Enayati and Salehi [17] have also reported on the structural evolution during the MA of $Fe_{75}Al_{25}$ and $Fe_{50}Al_{50}$ in a high-energy planetary ball mill under a specific condition. They reported that the MA of $Fe_{75}Al_{25}$ and $Fe_{50}Al_{50}$ initially produced a fine Fe/Al layered microstructure which later transformed directly to the corresponding intermetallic compounds, Fe_3Al and FeAl on further milling. Nayak et al. [18] reported the MA of $Al_{100-x}Fe_x$, (x = 2.5, 5, 10, 15 and 20) alloys. They reported that no other phase could be formed other than the formation of a supersaturated solution of Fe in Al in the case of Al–(2.5–10) %Fe alloys, while Al–20%Fe alloy formed nanocrystalline

metastable Al_5Fe_2 phase. Bonetti et al. [19] reported the MA behavior of $Fe_{75}Al_{25}$ powder mixture in a high-energy ball mill. They reported the extended solid solution of Al in Fe after 1 h of milling, and according to them, no amorphization reaction occurred even after 32 h of MA. Thermal analysis of the milled powder showed that Fe(Al) solid solution transformed to the disordered Fe_3Al and FeAl intermetallic compounds.

Among all the methods used for the synthesis of nanostructured Fe–Al intermetallic compound, MA is the most popular method. This solid state technique is especially useful for the fabrication of those compounds that are difficult to prepare by conventional processes due to high vapor pressure and large differences in melting point of components. Apart from this during MA synthesis takes place at room temperature. However, MA has few drawbacks like long period of milling and contamination from the atmosphere or milling media [20–22]. Here, the synthesis of the Fe_3Al intermetallic compound by MA has been investigated. The structural evolution of the Fe_3Al intermetallic compound, during the MA of $Fe_{75}Al_{25}$ for 40 h followed by isothermal annealing, was analyzed. Emphasis was given to find out the diffusion process of Al in Fe during the formation of Fe_3Al intermetallic compound by milling.

2 Experimental

Elemental Fe powder having purity 99% and elemental Al powder having purity >99.99 were procured from Loba Chemie. These powder mixtures were first blended in a stoichiometric ratio of $Fe_{75}Al_{25}(Fe_3Al)$. The mechanical alloying of $Fe_{75}Al_{25}$ powder mixture was carried out using a Fritsch P5 high-energy planetary ball mill operating at 300 rpm for 40 h. The vials and balls were made up of hardened chrome steel. The diameter of the balls was 10 mm, and the ball-to-powder weight ratio was maintained at 10:1. To minimize welding of powders during milling, toluene (C_7H_8) was used as a process controlling agent (PCA). Figure 2 is a schematic representation of the mechanical alloying (MA) process.

The isothermal annealing of the mechanically alloyed $Fe_{75}Al_{25}$ powder was carried out at a temperature 1100 °C for 2 h in the presence of Ar atmosphere in a tubular furnace. The structural evolution and the formation of phases taking place during ball milling and subsequent heat treatment of the ball milled powder were determined using X-ray diffraction (XRD). XRD of the various milled, as well as annealed samples, was done using a Philips Panalytical PW 3040/00 X-ray diffractometer with Cu K_α radiation ($\lambda = 1.5409$ Å) where Ni was used as a filter. The crystallite size and r.m.s. lattice strain were calculated from the broadening of the XRD peaks using Williamson-Hall equation. Precise lattice parameter was determined using the Nelson-Riley function. Differential scanning calorimetry and thermogravimetric analysis (DSC/TGA) was carried out using a Netzsch STA 409C simultaneous thermal analyzer at a heating rate of 10 °C/min in Ar atmosphere to determine the thermal stability of the various samples. The morphology of the milled powder and the annealed samples was analyzed using a JEOL-JSM-6480LV scanning electron microscope (SEM) enabled with energy-dispersive X-ray (EDX) analysis system. The milled powder was also analyzed using a JEOL JEM-2100 high-resolution transmission electron microscope (HRTEM) at an acceleration voltage of 200 keV.

3 Results and discussion

The SEM images in Fig. 3 show the particle morphology of the as-received Fe and Al powders used for the synthesis of Fe_3Al by mechanical alloying (MA). The SEM images of the as-received Fe powder in Fig.3a, b show Fe particles having a wide range of sizes. Very large Fe particles having size more than 70 μm and fine Fe particles having size <30 μm could be seen in the SEM images. The EDX analysis of the Fe particles along with the SEM image in Fig. 3b suggests that the composition of the particles is 100% Fe showing no contamination. From the SEM images of the as-received Al powder in Fig. 3c, d, it is evident that most of the Al particles are nearly spherical. Few particles were also found to be dumbbell shaped. The as-received Al powder consists of very fine equiaxed Al particles having a diameter of around 25 μm as well as elongated particles having lengths of up to 60 μm. The EDX analysis along with the SEM image in Fig. 3d suggests that the composition of the as-received powder is 100% Al.

The structural evolution of the $Fe_{75}Al_{25}$ powder during MA and subsequent isothermal annealing was analyzed using XRD. Elemental Fe and Al powder was taken in the stoichiometric ratio of 3:1 and milled for up to 40 h. Figure 3a shows the XRD pattern of $Fe_{75}Al_{25}$ powder after different intervals of milling time. Here, mechanical alloying (MA) has been carried out in hardened chrome steel milling media. As Fe is comparatively much softer than hardened chrome steel, contamination during milling due to the wear of the milling media has not been observed. The XRD patterns in Fig. 4a show that the Al(200) and Al(220) peaks are superposing with Fe(110) and Fe(200) peaks, respectively. However, all the diffraction peaks of Al with odd Miller indices such as (111) and (311) peaks are seen clearly as independent peaks. After milling for 4 h, the diffraction peaks of Al(111) and Al(311) disappeared due to peak broadening. The broadening of the XRD peaks with the increasing milling time can be attributed to the reduction in crystallite size and an increase in lattice strain. With the progress of milling, the three lead-

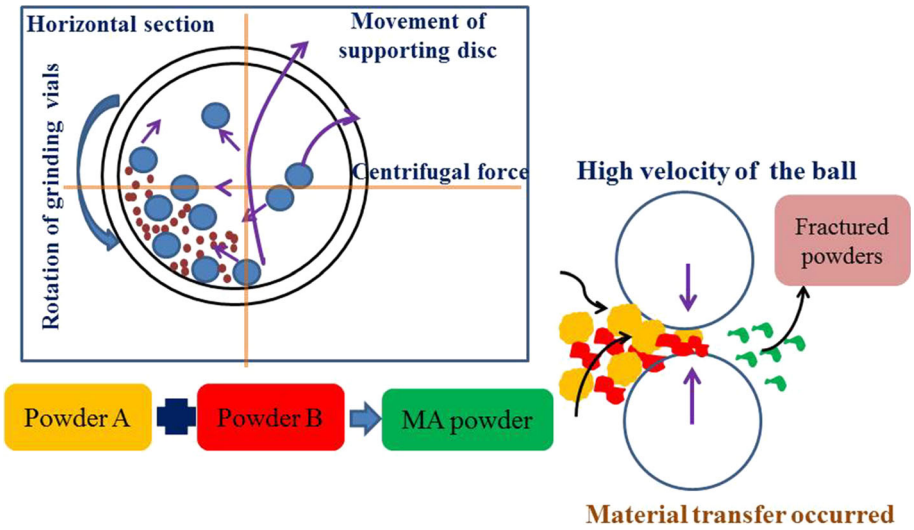

Fig. 2 Schematic representation of the mechanical alloying (MA) process

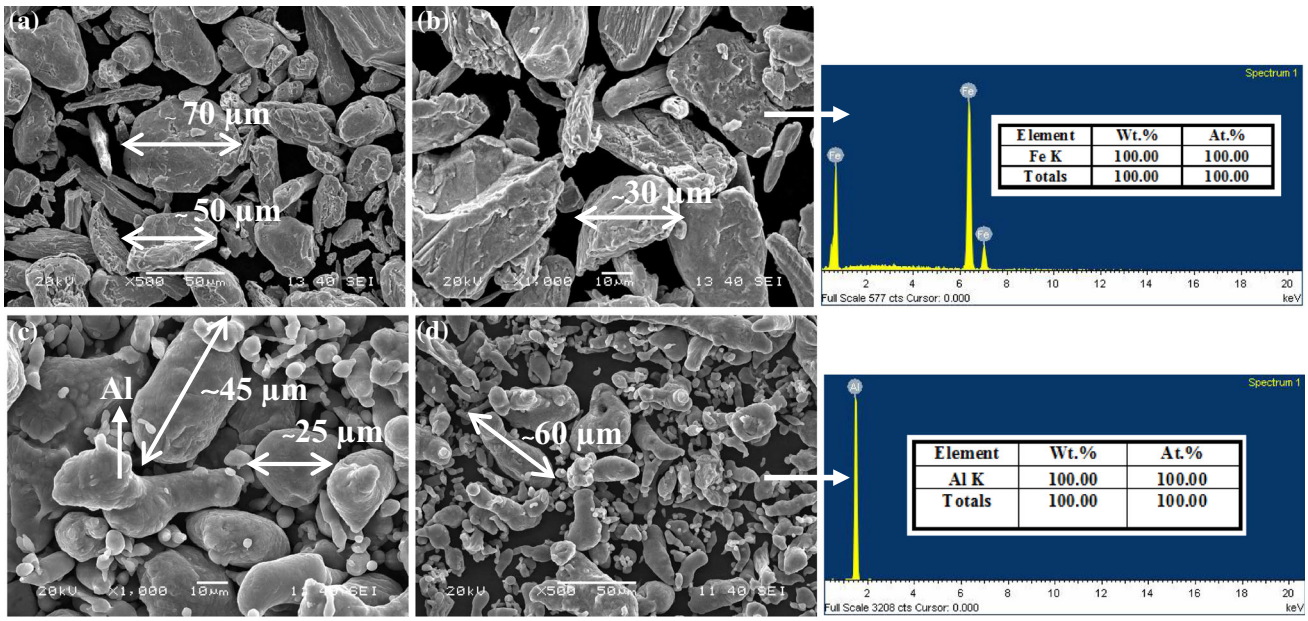

Fig. 3 SEM images of **a**, **b** as-received Fe powder and **c**, **d** as-received Al powder along with EDX analysis

ing diffraction peaks of Fe, namely, (110), (200) and (211), shifts toward lower diffraction angle which indicates the diffusion of Al atoms in the Fe lattice [23,24]. The shift in the Fe(110) peak toward lower 2θ values is clearly seen in the XRD plots of the various milled powders in the 2θ range of 43-47° shown in Fig. 4b. The variation of the crystallite size and the lattice strain of the Fe(Al) solid solution is shown in Fig. 5a, b, respectively. From the variation of the crystallite size and the lattice strain, it can be concluded that both the crystallite size and lattice strain vary in a similar manner with the progress in milling time. On prolonged milling, the lattice strain shows an increase.

Precise lattice parameter was determined by using the Nelson-Riley function [24]. Figure 6 shows the variation of the lattice parameter of Fe with the increase in milling time of $Fe_{75}Al_{25}$ powder. After 4 h of milling, the lattice parameter of Fe was found to be 2.87 Å, which is slightly more than that of the unmilled pure Fe (2.866 Å). It can be concluded that after about 4 h of milling the diffusion of Al in Fe takes place forming a solid solution of Al in Fe, that is, Fe(Al). Since the metallic radius of Al atoms (1.43 Å) is larger than the metallic radius of Fe atoms (1.24 Å), so the solid solution of Al in Fe lattice leads to an increase in the lattice parameter of Fe. The lattice parameter of Fe(Al) is more than that of pure Fe after diffusion of Al, having a larger atomic radius, into the Fe lattice. After 40 h of milling the lattice parameter of Fe(Al) was found to be around 2.92 Å. A similar sudden rise in the lattice parameter of Fe during milling of Fe–28Al

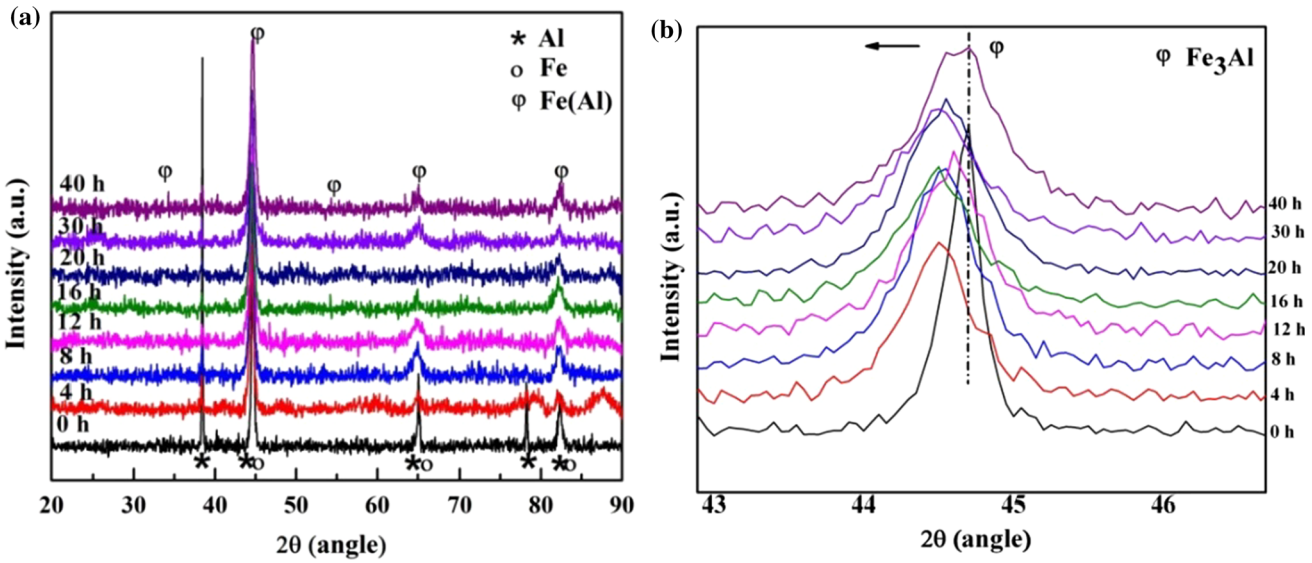

Fig. 4 **a** XRD pattern of $Fe_{75}Al_{25}$ powder after different interval of milling time. **b** XRD pattern of $Fe_{75}Al_{25}$ powder in the 2θ range of 43°–47°

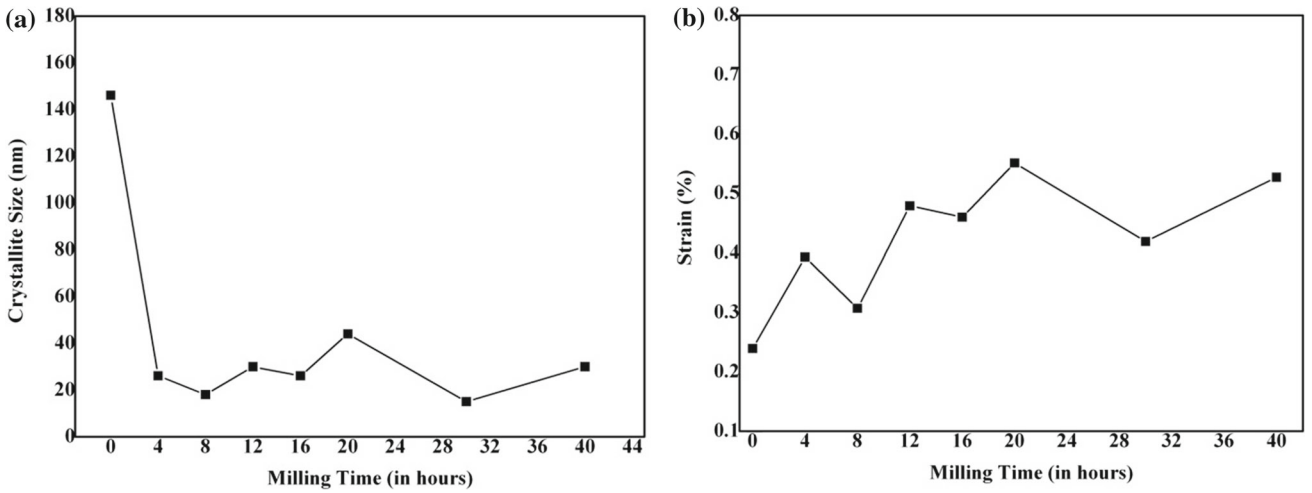

Fig. 5 Variation of **a** crystallite size and **b** lattice strain of mechanically alloyed $Fe_{75}Al_{25}$ powder with milling time

powder was also reported by Talischi and Samadi [25] and also by Tang et al. [26].

Figure 7 shows the XRD plots of commercially available Fe_3Al powder, 40-h milled $Fe_{75}Al_{25}$powder, and 40-h milled $Fe_{75}Al_{25}$powder heat-treated at 1100 °C for 2 h in Ar atmosphere. The XRD pattern of both commercially available Fe_3Al powder and the Fe_3Al powder developed by MA and subsequent annealing of the milled powder shows the (220), (400) and (422) diffraction peaks of Fe_3Al at around 44°, 64° and 82°, respectively. During annealing, the order transformation of the disordered Fe(Al) solid solution formed after 40 h of milling of $Fe_{75}Al_{25}$ to the ordered $D0_3$-Fe_3Al took place. The presence of the (111) superlattice peak of $D0_3$-Fe_3Al in the XRD pattern is a direct evidence of the ordered arrangement in the alloy. The small, weak peak which is present along with the fundamental lines at around $2\theta = 25.65°$ can be indexed as the (111) superlattice peak of $D0_3$-Fe_3Al. The (111) superlattice peak could also be seen in XRD spectra of both the commercially available Fe_3Al powder as well as the Fe_3Al synthesized by MA followed by isothermal annealing at around 26°. Along with the Fe_3Al peaks, few diffraction peaks corresponding to FeAl having very low peak intensity could also be seen in the XRD plot at 2θ values of around 35° and 55° [27].

The SEM images in Fig. 8a–h show the structural evolution of the $Fe_{75}Al_{25}$ powder after different periods of milling. During the initial period of milling, flake-like particles could be seen as is evident from the SEM images in Fig. 8b, c. During MA, the powder was subjected to high-energy collision, which causes plastic deformation, cold welding and fracture.

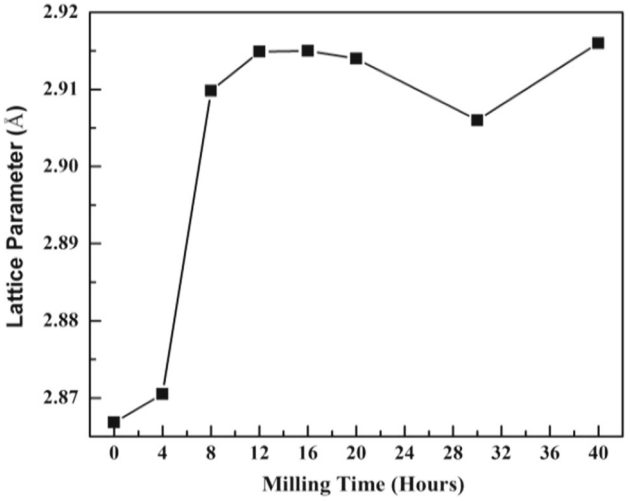

Fig. 6 Variation of lattice parameter of Fe in mechanically alloyed $Fe_{75}Al_{25}$ powder

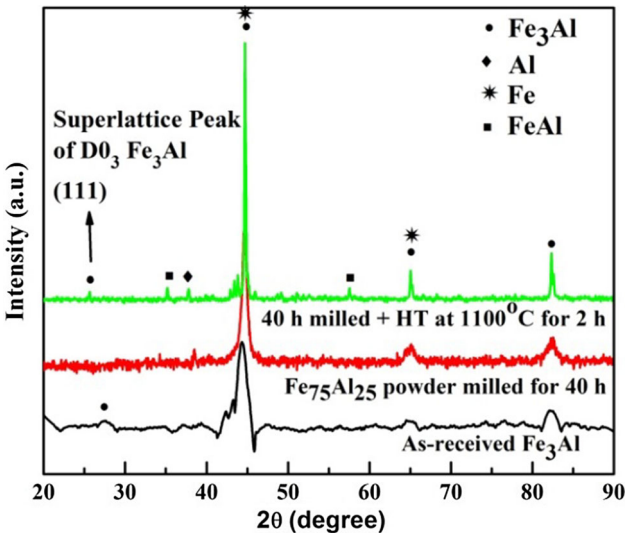

Fig. 7 X-ray diffraction plots of **a** commercially available Fe_3Al, **b** $Fe_{75}Al_{25}$ powder milled for 40 h, **c** $Fe_{75}Al_{25}$ powder milled for 40 h and heat-treated at 1100 °C for 2 h

With the increase in milling time, the extent of further plastic deformation decreases. This is evident from the SEM images in Fig. 8d–f. As welding is the dominant mechanism during MA, the morphology of the particles changes to agglomerates of flattened particles. Layered composite powder particles consisting of various combinations of the starting ingredients are formed. In the case of soft and ductile metal powders, the flattened layers overlap and form cold welds. To reduce cold welding between the powder particles, toluene was used as a process controlling agent. At the same time, the work-hardened metal powder particles continue to fracture. In the final stages of milling, the competing events of cold welding and fracturing continue repeatedly. As a result, a refined and homogenized microstructure is obtained after around 30 h of milling [27,28]. After around 30 h of MA, the shape of the powder particles also become more regular as is evident from the SEM image in Fig. 8h.

Figure 9a–d shows the HRTEM images of the 40-h milled $Fe_{75}Al_{25}$ powder. From the HRTEM images, it is evident that ultrafine particles having a size <100 nm could be achieved after 40 h of milling of the $Fe_{75}Al_{25}$ powder. Fringes could be seen at the edges of the nanoparticles developed after 40 h of milling (Fig. 9a inset). The d spacing of the (110) planes in the Fe(Al) nanoparticles as calculated from the XRD spectra of the 40-h milled $Fe_{75}Al_{25}$ powder (Fig. 7) using the Bragg's law was found to be around 0.202 nm which is in close agreement with the d spacing reported in literature of 0.205 nm [27]. The SAD pattern in Fig. 9e shows sharp concentric rings which could be indexed to the (110), (200) and (211) diffraction planes of Fe and corresponds to that of Fe(Al) [29,30].

Figure 10 shows the SEM image and the elemental maps of Al and Fe in the $Fe_{75}Al_{25}$ powder milled for various periods of time. It shows the distribution of Fe and Al elements and the compositional changes with the progress in milling time. The elemental maps of Al and Fe after different periods of milling of the $Fe_{75}Al_{25}$ powder have been analyzed to determine the mechanism of the formation of Fe(Al) solid solution. The alloying during the milling of $Fe_{75}Al_{25}$ powder is governed by the diffusion of the Al atoms into the Fe lattice because of the higher diffusion coefficient of the Al atoms in the Fe lattice compared with that of the Fe atoms in the Al lattice [30,31]. Furthermore, the solid solubility of Al in Fe is enhanced due to the increase in defects in the Fe lattice and the decrease in the Fe grain size during milling. Before the start of milling, distinct large sized Fe (green color) and Al (red color) particles are observed in Fig. 10a. However, after 4 h of MA diffusion of Al atoms into Fe lattices is seen in Fig. 10b and with the progress of milling Al (red color) is seen dispersed within the Fe (green color) particles. This clearly suggests that with the progress in milling time gradual diffusion of Al takes place into the Fe particles leading to the formation of Fe(Al) solid solution. During the initial stages of milling (up to 4 h), the deformation of the Fe and Al particles mainly takes place. Both the components Fe and Al are inhomogeneously distributed, and the alloying between Fe and Al is weak during this period. This is also evident from Fig. 4 which shows only a slight increase in the lattice parameter of Fe within the initial 4 h of milling. This is possibly due to the lower amount of the Fe and Al grain boundaries and the low defect concentration in the $Fe_{75}Al_{25}$powder during the initial period of milling which has also been reported by Tang et al. [26]. From the elemental maps of Al and Fe in Fig. 10 it can be found that during the initial stages of milling the Al particles are deformed and surround the Fe particles constructing composite particles. Thereafter, the composite particles aggregate and weld. After about 12 h of MA,

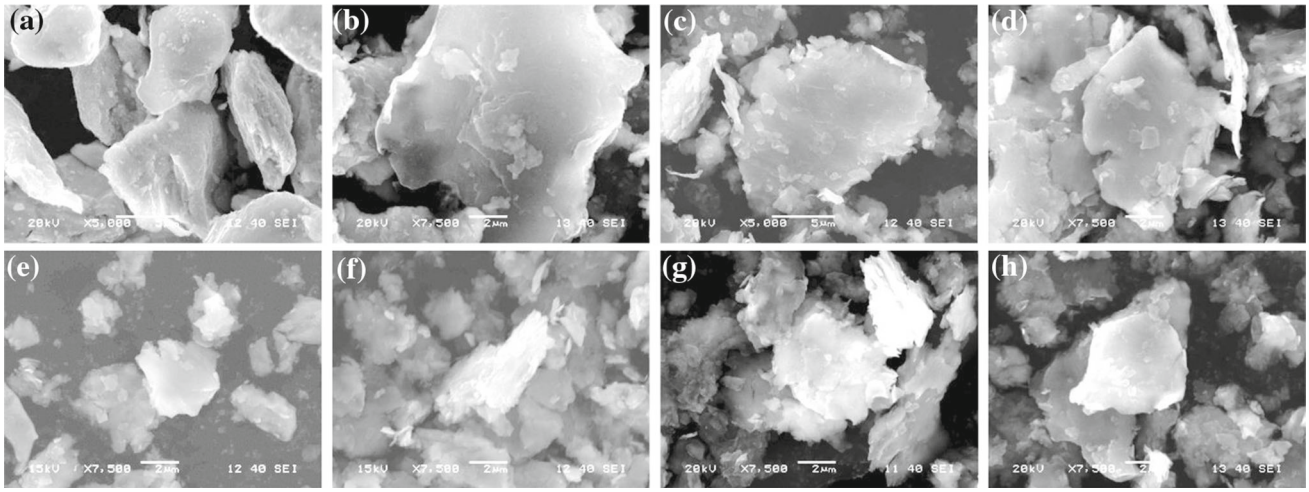

Fig. 8 SEM images of mechanically alloyed $Fe_{75}Al_{25}$ powder after **a** 0 h, **b** 4 h, **c** 8 h, **d** 12 h, **e** 16 h, **f** 20 h, **g** 30 h, **h** 40 h of milling

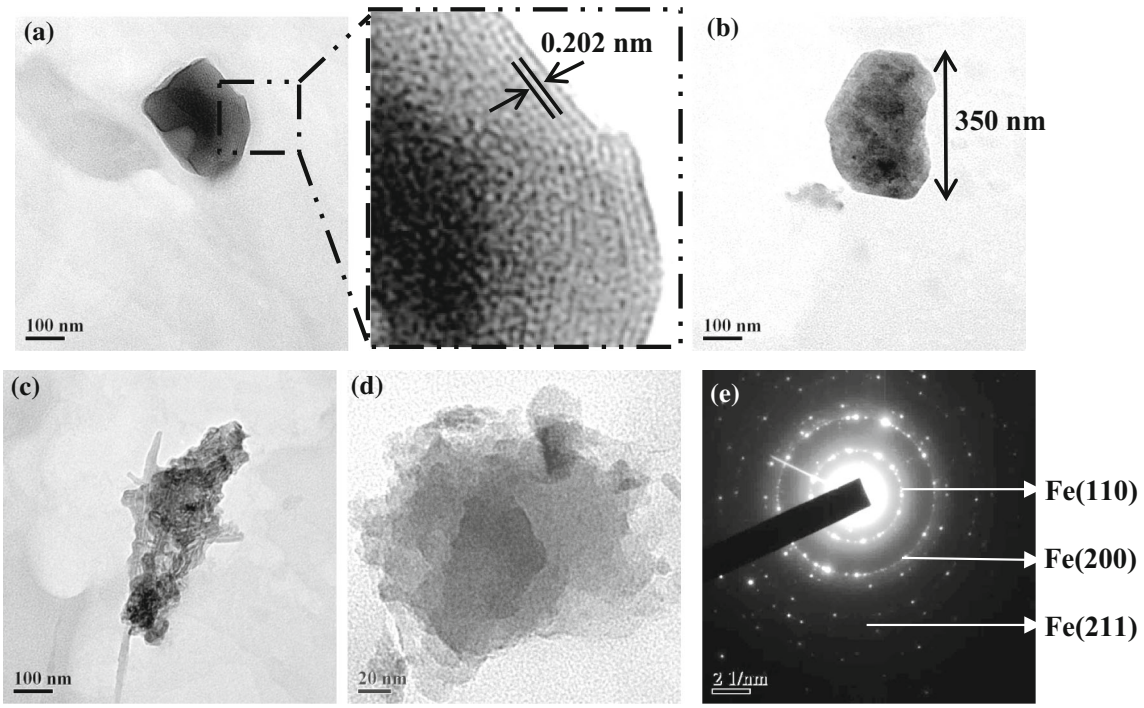

Fig. 9 **a–d** HRTEM images, **e** SAD pattern of 40-h mechanically alloyed $Fe_{75}Al_{25}$ powder

complete diffusion of Al into Fe and homogenization of the composite particles take place resulting in the formation of Fe(Al) solid solution. With further milling, it could be clearly noticed from the elemental maps that both the components, Fe and Al, are well distributed resulting in the formation of homogeneous Fe(Al) solid solution. The EDX analysis given along with the SEM images in Fig. 10 shows the composition of the particles during milling. The EDX analysis of the particles shows a gradual increase in the at.% of Al in the particles from 7.73 at.% after 4 h of milling to 28 at.% after 40 h of milling. It should be noted that Fe_3Al has 25 at.% Al and 75 at.% Fe and the particles in Fig. 10h of the 40-h milled $Fe_{75}Al_{25}$ powder show a composition of 28 at.% Al and 72 at.% Fe. With the increase in milling time, the distribution of Al in Fe was continuously increasing. Therefore, it can be concluded that a homogeneous alloy is formed by dissolving an atom species into another where both the species of atoms are distributed over the crystal lattice positions [33,34].

Figure 11a shows the DSC analysis of the 40-h milled $Fe_{75}Al_{25}$ powder. The DSC plot of 1-h and 4-h milled $Fe_{75}Al_{25}$ powder shows an endothermic peak at around 662 °C. This is due to the melting of the residual Al in the milled powder. Al has a melting point of 660 °C. As all the Al has not diffused in the Fe lattice to form Fe(Al) solid solution

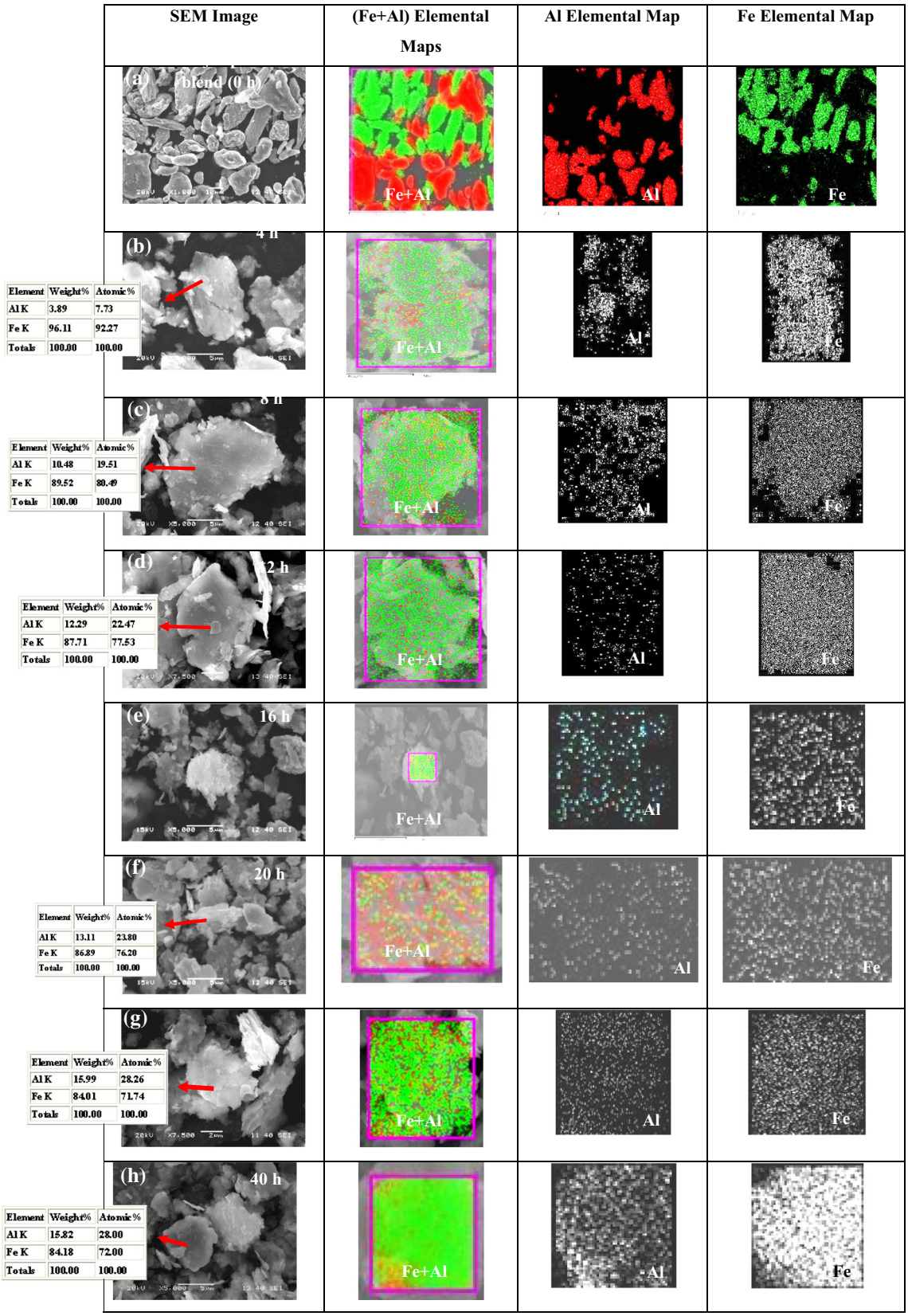

Fig. 10 SEM image and elemental maps of (Al + Fe) combined, Al and Fe of $Fe_{75}Al_{25}$ powder milled for **a** 0 h, **b** 4 h, **c** 8 h, **d** 12 h, **e** 16 h, **f** 20 h, **g** 30 h, and **h** 40 h

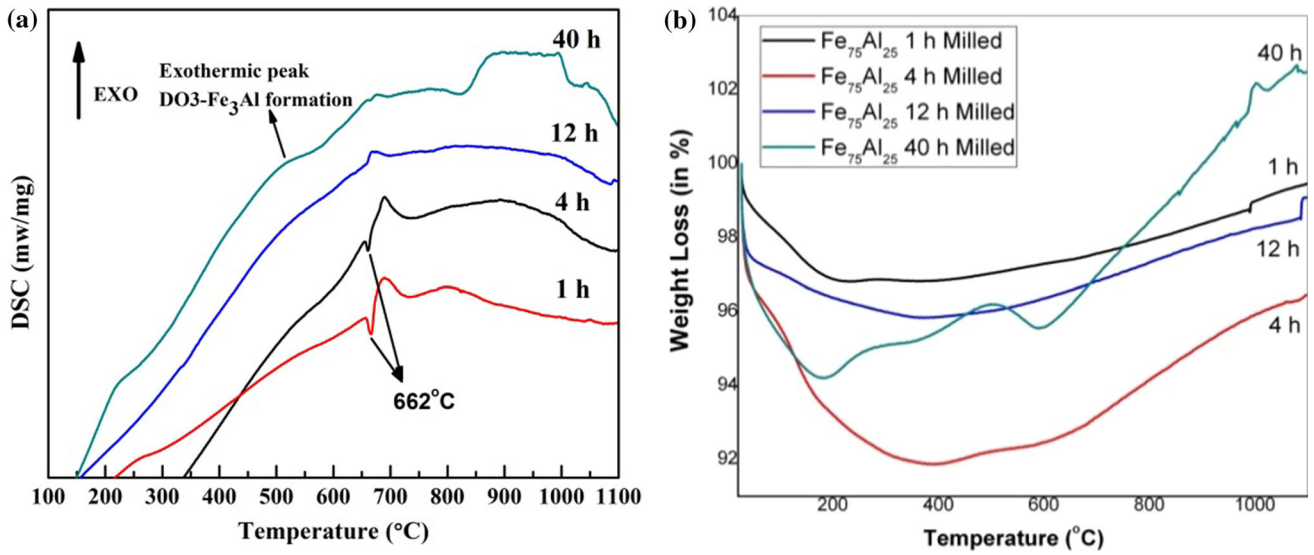

Fig. 11 **a** DSC and **b** TGA of $Fe_{75}Al_{25}$ powder milled for various periods of time

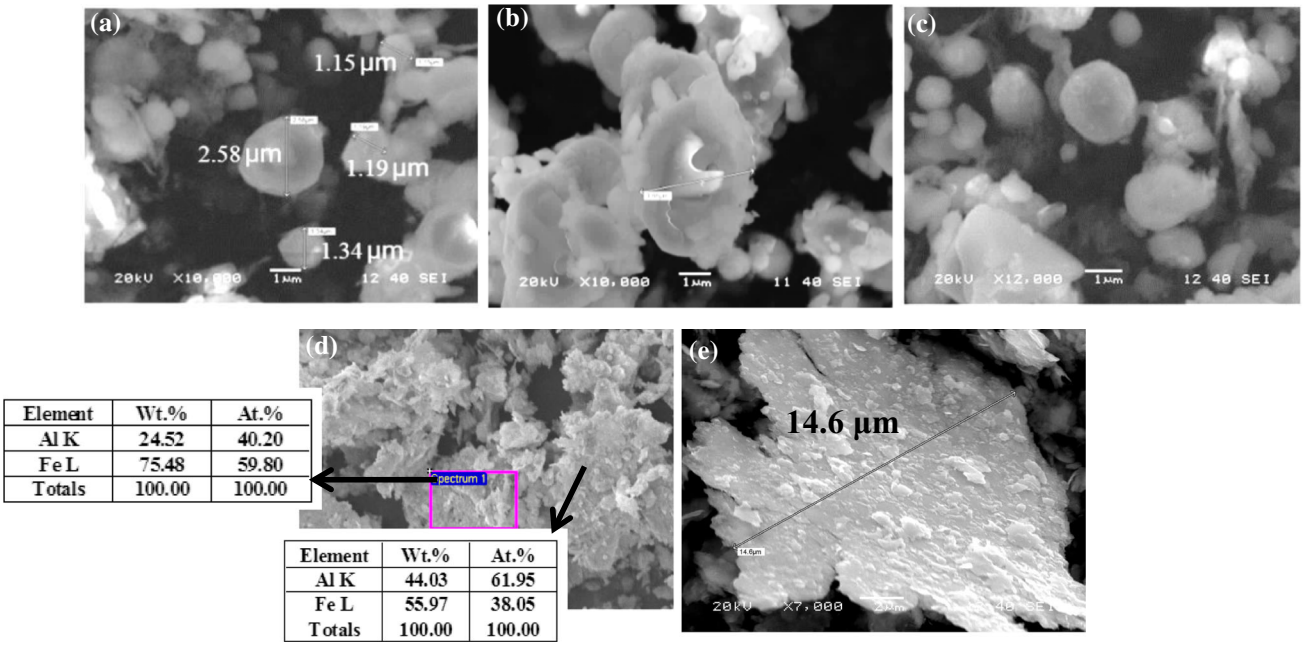

Element	Wt.%	At.%
Al K	24.52	40.20
Fe L	75.48	59.80
Totals	100.00	100.00

Element	Wt.%	At.%
Al K	44.03	61.95
Fe L	55.97	38.05
Totals	100.00	100.00

Fig. 12 SEM images of 40-h mechanically alloyed $Fe_{75}Al_{25}$ powder heat-treated at 1100 °C for 2 h along with EDX analysis

during the initial period of milling, some amount remains in the milled powder as residual Al. However, the endothermic peak at around 662 °C is not visible in the DSC plots of the 12-h and 40-h milled powder. This suggests that a significant amount of Al has dissolved into the Fe lattice after 40 h of milling and forming a complete Fe(Al) solid solution. A shallow exothermic peak seen at around 500 °C in the DSC plot of the 40-h milled $Fe_{75}Al_{25}$ powder is due to the formation of the ordered $D0_3$-Fe_3Al. Ordered $D0_3$-Fe_3Al could be formed from the 40-h milled $Fe_{75}Al_{25}$ powder when heated to a temperature above 500 °C. Qj et al. [32] have also reported that the formation temperature of nano-Fe_3Al is estimated at a temperature of around 587 °C through DSC test under Ar atmosphere. The binary Fe–Al phase diagram in Fig. 1a also indicates that the $D0_3$-Fe_3Al phase is stable up to a temperature of about 600 °C. So the formation temperature for intermetallic compound $D0_3$-Fe_3Al during isothermal annealing is also expected to be below 600 °C [17,20,35]. The initial loss of mass up to the temperature below 200 °C shown in the TGA plots of all the $Fe_{75}Al_{25}$ powders milled for various periods of time in Fig. 11b is due to the evaporation of the absorbed toluene which was used as a process con-

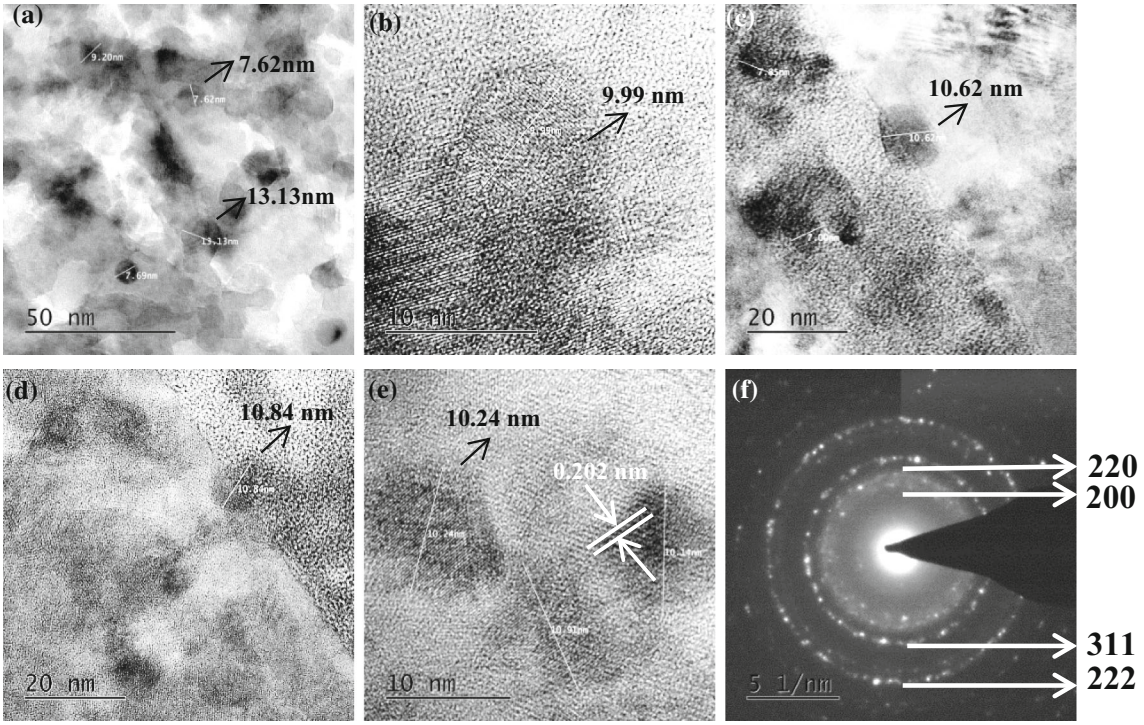

Fig. 13 **a–e** HRTEM images and **f** SAD pattern of 40-h mechanically alloyed $Fe_{75}Al_{25}$ powder heat-treated at 1100 °C for 2 h

trolling agent (PCA) during the mechanical alloying (MA) process. A slight rise in mass could be seen beyond 200 °C in all the TGA plots which can be attributed to the oxidation of the milled powder. The highest rise in mass is seen in the case of the 40-h milled $Fe_{75}Al_{25}$ powder as the 40-h milled powder is more susceptible to oxidation due to the high surface energy of the 40-h milled nanocrystalline powder.

Figure 12a–e shows the SEM images of the 40-h mechanically alloyed $Fe_{75}Al_{25}$powder heat-treated at 1100 °C for 2 h along with the EDX analysis of the particles. By comparing the SEM images in Figs. 8h and 12, it is evident that the flake-like milled powder particles formed after 40 h of milling of $Fe_{75}Al_{25}$ powder changes to spherical shaped particles after subsequent heat treatment. The spherical particles have a diameter in the range of around 0.5–4 μm. Flattened Al particles which remained free and did not dissolve into the Fe particles could also be seen in the SEM micrographs as shown in Fig. 12e. As pure Al is very ductile, it could be easily flattened during milling. It should be noted that Fe_3Al being an intermetallic compound is very brittle and could be reduced to very fine size during milling as could be seen in the SEM images in Fig. 12a–c. The EDX analysis of a particle in Fig. 12d shows a composition of 61.95 at.% Fe and 38.05 at.% Al. This is very close to the composition of Fe_3Al, which has a composition of 75 at.% Fe and 25 at.% Al.

Figure 13a–e shows the HRTEM images of the 40-h mechanically alloyed $Fe_{75}Al_{25}$powder heat-treated at 1100 °C for 2 h along with the SAD pattern in Fig. 13f. The HRTEM images clearly show nanoparticles having a size in the range of 9–14 nm. Atomic fringes of the Fe_3Al nanocrystals are clearly visible in the HRTEM images in Fig. 13b, e which clearly indicates the formation of the Fe_3Al intermetallic compound. The SAD pattern in Fig. 13f shows sharp concentric rings which are a direct evidence of the nanocrystalline nature of the powder [36].

4 Conclusions

Fe_3Al intermetallic compound could be synthesized by mechanical alloying (MA) of $Fe_{75}Al_{25}$ powder for 40-h followed by isothermal heat treatment of the milled powder at 1100 °C for 2 h in Ar atmosphere. The XRD analysis of the 40-h milled $Fe_{75}Al_{25}$ powder shows peaks corresponding to Fe(Al) solid solution along with peaks Fe and Al. The (111) superlattice peak at 2θ of around 25.65° in the XRD analysis of the heat-treated powder confirmed the formation of the ordered $D0_3$-Fe_3Al intermetallic compound. A shallow exothermic peak below 600 °C in the DSC plot of the 40-h milled powder also confirms the formation of ordered $D0_3$-Fe_3Al. This suggests that a significant amount of Al has dissolved after 40 h of milling forming a complete solid solution. The elemental maps of Al and Fe in the $Fe_{75}Al_{25}$ powder milled for various periods of time suggest the gradual diffusion of Al in the Fe particles. The EDX analysis of the $Fe_{75}Al_{25}$ powder milled for various periods of time also

confirms the gradual increase in Al concentration in the Fe particles. The final concentration of Al in the Fe particle after 40 h of milling of $Fe_{75}Al_{25}$ powder was found to be around 28 at.%. The HRTEM images confirmed that the Fe_3Al synthesized by MA is <15 nm in size. Atomic fringes of the Fe_3Al nanocrystals are clearly visible in the HRTEM images indicating the formation of Fe_3Al intermetallic compound.

Acknowledgements We gratefully acknowledge the support provided by the XRD, SEM and thermal analysis laboratories of Metallurgical and Materials Engineering Department and the FESEM laboratory of the Ceramic Engineering Department, NIT Rourkela. We also thank the support provided by Chemical Engineering Department, NIT Rourkela, for helping us in analyzing our samples using the HRTEM. We would like to gratefully acknowledge the support provided by Central Research Facility, IIT Kharagpur.

References

1. Benjamin, J.S.: Dispersion strengthened superalloys by mechanical alloying. Metall. Mater. Trans. A **1**, 2943 (1970)
2. Angelo, P.C.; Subramanian, R.: Powder Metallurgy: Science, Technology and Applications. PHI Learning Pvt. Ltd., New Delhi (2008)
3. Balci, Q.; Agogullari, D.; Gokce, H.; Duman, I.; Ovecoglu, M.L.: Influence of TiB_2 particle size on the microstructure and properties of Al matrix composites prepared via mechanical alloying and pressureless sintering. J. Alloys Compd. **586**, S78–S84 (2014)
4. Venkateswaran, K.; Kamaraj, M.; Rao, P.K.: Dry sliding wear of a powder metallurgy copper-based metal matrix composite reinforced with iron aluminide intermetallic particles. J. Compos. Mater. **4**(14), 1713–1728 (2007)
5. Velasco, F.; Da Costa, C.E.; Torralba, J.M.: Mechanical properties and wear behaviour of PM aluminium composite reinforced with Fe_3Al particles. Powder Metall. **45**, 247 (2002)
6. Farrokhi, A.; Samadi, A.; Asadabad, M.A.; Talischi, L.A.: Characterization of mechanically alloyed nano structured Fe_3Al intermetallic compound by X-ray diffractometry. Adv. Powder Technol. **26**, 797 (2015)
7. Bonetti, E.; Scipione, G.; Valdrf, G.; Enzo, S.; Frattini, R.; Macri, P.P.: A study of nanocrystalline iron and aluminium metals and Fe_3Al intermetallic by mechanical alloying. J. Mater. Sci. **30**, 2220–2226 (1995)
8. Adabavazeh, Z.; Karimzadeh, F.; Enayati, M.H.: Synthesis and structural characterization of nanocrystalline $(Ni,Fe)_3Al$ intermetallic compound prepared by mechanical alloying. Adv. Powder Technol. **23**, 284 (2012)
9. Li, J.; Liu, Q.; Shi, R.X.; Wen, Y.; Yin, Y.S.: Preparation and mechanical properties of $Fe_3Al(Ti)$/Tic composites. J. Mater. Process. Technol. **208**, 105–110 (2008)
10. Wang, J.; Xing, J.; Qiu, Z.; Zhi, X.; Cao, L.: Effect of fabrication methods on microstructure and mechanical properties of Fe_3Al based alloys. J. Alloys Compd. **488**(1), 117–122 (2009)
11. Jiang, T.: Investigation of microstructure and property of Fe_3Al/Al_2O_3 composites. Adv. Mater. Res. **150–151**, 1409–1412 (2011)
12. Panda, D.; Kumar, L.; Alam, S.N.: Development of Al-Fe_3Al nanocomposite by powder metallurgy route. Mater. Today Proc. **2**, 3565 (2015)
13. Mitra, R.: Structural Intermetallics and Intermetallic Matrix Composites. CRC Press, Boca Raton (2015)
14. Westbrook, J.H.; Fleischer, R.L.: Intermetallic Compounds, Principles and Practice. Wiley, New York (2002)
15. Murty, B.S.; Ranganathan, S.: Novel materials synthesis by mechanical alloying/milling. Int. Mater. Rev. **43**(3), 101–141 (1998)
16. Oleszak, D.; Shingu, P.H.: Mechanical alloying in the Fe–Al system. Mater. Sci. Eng. A **181–182**, 1217–1221 (1994)
17. Enayati, M.H.; Salehi, M.: Formation mechanism of Fe_3Al and FeAl intermetallic compounds during mechanical alloying. J. Mater. Sci. **40**, 3933–3938 (2005)
18. Nayak, S.S.; Wollgarten, M.; Banhart, J.; Pabi, S.K.; Murty, B.S.: Nanocomposites and an extremely hard nanocrystalline intermetallic of Al–Fe alloys prepared by mechanical alloying. Mater. Sci. Eng. A **527**, 2370–2378 (2010)
19. Bonetti, E.; Valdre, G.; Enzo, S.; Cocco, G.; Soletta, I.: Nanostructured Fe_3Al intermetallic obtained by mechanical alloying and thermal ageing. Nanostruct. Mater. **2**, 369 (1993)
20. Stoloff, N.S.: Physical Metallurgy and Processing of Intermetallic Compounds. Chapman & Hall, New York (1996)
21. Kainer, K.U.: Basics of Metal Matrix Composites. Wiley-VCH Verlag GmbH & Co. KGaA, Weinheim (2006)
22. Schwarz, R.B.; Koch, C.C.: Formation of amorphous alloys by the mechanical alloying of crystalline powders of pure metals and powders of intermetallics. Appl. Phys. Lett. **49**(3), 146–148 (1986)
23. Suryanarayana, C.; Norton, M.G.: X-ray Diffraction: A Practical Approach. Springer, New York (1998)
24. Cullity, B.D.; Stock, S.R.: Elements of X-ray Diffraction, 3rd edn. Pearson Education Limited, London (2014)
25. Talischi, L.A.; Samadi, A.: Structural characterization and ordering transformation of mechanically alloyed nanocrystalline Fe–28Al powder. J. Ultrafine Grained Nanostruct. Mater. **49**(2), 112–119 (2016)
26. Tang, W.M.; Zheng, Z.X.; Tang, H.J.; Ren, R.; Wu, Y.C.: Structural evolution and grain growth kinetics of the Fe–28Al elemental powder during mechanical alloying and annealing. Intermetallics **15**, 1020–1026 (2007)
27. Jiang, H.G.; Perez, R.J.; Lau, M.L.: Formation kinetics of nanocrystalline Fe–4 wt% Al solid solution during ball milling. J. Mater. Res. **12**, 1429–1432 (1997)
28. Chen, S.; Chen, Y.; Tang, Y.; Luo, B.; Yi, Z.; Wei, J.; Sun, W.: Synthesis and characterization of FeAl nanoparticles by flow-levitation method. J. Cent. South Univ. **20**, 845 (2013)
29. Rosas, G.; Patiño-Carachure, C.; Tellez, O.; Reyes-Gasga, J.: Electron microscopy and X-ray diffraction characterization of FeAl-BN nanocomposites produced by mechanical alloying. Acta Microsc. **19**, 285 (2010)
30. Olszówka-Myalska, A.; Maziarz, W.: Microstructural analysis of iron aluminide formed by self-propagating high-temperature synthesis mechanism in aluminium matrix composite. J. Microsc. **224**, 1 (2006)
31. White, R.L.: The use of mechanical alloying in the manufacture of multi filamentary superconductor wire. Ph.D. Thesis, Stanford University, USA (1979)
32. Qj, N.; Hu, M.; Wang, Z.; Lu, Z.; Xie, C.: Synthesis of Al-Fe_3Al core-shell intermetallic nanoparticles by chemical liquid deposition method. Adv. Powder Technol. **4**, 926 (2013)
33. Koch, C.C.: Intermetallic matrix composites prepared by mechanical alloying—a review. Mater. Sci. Eng. A **244**, 39 (1998)
34. Liu, Z.G.; Guo, J.T.; He, L.L.; Hu, Z.Q.: Formation of B2 intermetallic NiAl and FeAl by mechanical alloying. Nanostruct. Mater. **4**(7), 787–794 (1994)
35. Tu, J.P.; Meng, L.; Liu, M.S.: Friction and wear behavior of Cu-Fe_3Al powder metallurgical composites in dry sliding. Wear **220**(1), 72–79 (1998)
36. Pithawalla, Y.B.; El-Shall, M.S.; Deevi, S.C.: Synthesis and characterization of nanocrystalline iron aluminide particles. Intermetallics **8–9**, 1225 (2000)